Room-temperature coherent coupling of single spins in diamond

TORSTEN GAEBEL[1], MICHAEL DOMHAN[1], IULIAN POPA[1], CHRISTOFFER WITTMANN[1], PHILIPP NEUMANN[1], FEDOR JELEZKO[1]*, JAMES R. RABEAU[2], NIKOLAS STAVRIAS[2], ANDREW D. GREENTREE[3], STEVEN PRAWER[2,3], JAN MEIJER[4], JASON TWAMLEY[5], PHILIP R. HEMMER[6] AND JÖRG WRACHTRUP[1]*

[1]3. Physikalisches Institut, Universität Stuttgart, 70550 Stuttgart, Germany
[2]School of Physics, University of Melbourne, Melbourne, Victoria 3010, Australia
[3]Centre for Quantum Computer Technology, School of Physics, University of Melbourne, Melbourne, Victoria 3010, Australia
[4]Central Laboratory of Ion Beam and Radionuclides, Ruhr University, 44801 Bochum, Germany
[5]Centre for Quantum Computer Technology, Macquarie University, Sydney 2109, Australia
[6]Department of Electrical and Computer Engineering, Texas A&M University, Texas 77843-3128, USA
*e-mail: f.jelezko@physik.uni-stuttgart.de; j.wrachtrup@physik.uni-stuttgart.de

Published online: 28 May 2006; doi:10.1038/nphys318

Coherent coupling between single quantum objects is at the very heart of modern quantum physics. When the coupling is strong enough to prevail over decoherence, it can be used to engineer quantum entangled states. Entangled states have attracted widespread attention because of applications to quantum computing and long-distance quantum communication. For such applications, solid-state hosts are preferred for scalability reasons, and spins are the preferred quantum system in solids because they offer long coherence times. Here we show that a single pair of strongly coupled spins in diamond, associated with a nitrogen-vacancy defect and a nitrogen atom, respectively, can be optically initialized and read out at room temperature. To effect this strong coupling, close proximity of the two spins is required, but large distances from other spins are needed to avoid deleterious decoherence. These requirements were reconciled by implanting molecular nitrogen into high-purity diamond.

Strong coherent coupling between quantum objects is essential for applications in quantum information science. In addition, coupling to photons is also necessary for long-distance quantum communication applications. However, quantum systems with strong coupling to each other or to photons also tend to be strongly coupled to their environment, leading to decoherence. This is especially true for quantum objects in solid-state hosts. On the other hand, solids are preferred for many applications due to their relative ease of scaling. Phonons are one of the main sources of decoherence for solid-state quantum objects, and hence recent demonstrations of strong coherent coupling between optically active quantum systems have been done at low temperature[1,2]. An exception to this general rule is the nitrogen-vacancy (NV) defect in diamond. Since the discovery that the spin states of individual NV centres can be rapidly spin polarized[3] and read out optically with a confocal microscope[4], a number of quantum gate operations have been demonstrated, many at room temperature. These include Rabi nutations of single electron and nuclear spins, quantum process tomography as well as a complete two-qubit quantum gate demonstration using a NV-^{13}C 'molecule'[3,5,6]. As such there has been increasing interest in NV diamond for quantum computing, see for example recent reviews[7,8]. Single NV centres have also been investigated as a single-photon source for quantum communication applications[9]. Recently, the carving of optical microstructures in monolithic diamond has been demonstrated[10], which suggests that cavity quantum electrodynamics may be possible with NV centres[11,12]. The role of excess substitutional nitrogen (N) spins on the dephasing of NV centres has been studied in ensemble[13] and single-centre[14] work, confirming that N can act as the major source of decoherence. Thus to achieve a long coherence time, substitutional N must be eliminated from

the diamond host. However, without N there would be no NVs. Fortunately, NV centres can be created in diamond by single-ion implantation of nitrogen[15,16]. As this technique does not require the presence of nitrogen in the starting material, ultrapure (type IIa) diamond can be used as a substrate.

The structure of the NV colour centre is shown in Fig. 1a. It consists of a nitrogen and a vacancy in an adjacent lattice site. When the nitrogen is implanted, numerous vacancies are created which can be removed by annealing near 800 °C. During the annealing process, one of the mobile vacancies can become trapped by the implanted nitrogen to create an NV centre. If all of the N could be activated as NV, it would be possible to create an all-NV quantum computer. In the absence of 100% yield, a thorough investigation of the coupling dynamics between NV and N must be made to place limits on the degree of perfection that must be attained to build realistic devices. Alternatively, the coupling between a single N and a single NV centre can be used, as is done here, to build a quantum computer even in the absence of perfect yield.

The NV defect appears in two forms, neutral and negatively charged, and it is the negatively charged species that we are concerned with here. The ground state is an electron spin triplet ($S=1$)[17], which has been well-characterized in the ensemble limit[18]. The transition between ground and excited spin triplets has a large oscillator strength (0.12), which allows the optical detection of single NV defects. The energy-level structure of the NV defect pertinent to our experiments is shown in Fig. 1b. Although the structure of the excited-state spin depends on the local crystal environment, photon scattering normally preserves the spin of the $m_s=0$ state, whereas the $m_s=\pm1$ states can undergo a non-radiative decay to the $m_s=0$ state with some probability. This leads to rapid spin polarization of the NV by optical pumping, and also to a spin-dependent photon-scattering efficiency allowing readout of the electronic spin state by monitoring the photoluminescence intensity. This ability to optically orient and readout individual spin states at room temperature sets the NV apart from most solid-state spin systems. See ref. 19 for a discussion that explains these effects from considerations of the symmetry of the NV centres.

To verify the expected long spin-coherence time of the implanted defects, Fig. 1c shows a Hahn echo decay time of 350 μs from an individual defect, created by implanting ^{14}N atoms. This phase coherence time (T_2) is significantly longer than the previously reported ensemble value (50 μs for diamonds with very low nitrogen concentration[13]). Presumably, in the present case coupling to the ^{13}C nuclear spin remains a factor limiting the coherence time (the natural abundance of ^{13}C is 1.1%)[20]. The homogeneous linewidth of the ^{13}C nuclear magnetic resonance spectrum is 100 Hz at room temperature indicating an average spin flip-flop time of 10 ms (ref. 21). The electron spin experiences a change in the local field if a pair of nuclei changes its mutual spin configuration. Flip-flop processes are strongly suppressed when in close proximity to the NV centre, because the nuclei experience a strong hyperfine coupling induced energy shift with respect to the spin bath. The decoupling radius r is given by[22] $r=[2S(\gamma_e/\gamma_n)]^{1/4}a$, where S is the electron spin quantum number, γ_e and γ_n are the gyromagnetic ratios of electron and nuclear spins, and a is the average nearest-neighbour separation between nuclear spins. Substitution of $a=0.44$ nm for the natural 1.1% ^{13}C abundance yields the minimum radius of the frozen core to be 2.2 nm. This corresponds to random jumps of the electron spin resonance (ESR) frequency for the defect of about 2.5 kHz, which is in agreement with the experimentally observed phase coherence time. Hence, the availability of isotopically pure diamonds should lead to a further increase in T_2. In addition, the angular dependence of the dipolar coupling can be used to suppress decoherence by applying a properly oriented magnetic field[23]. Ultimately, the spin coherence time will be limited by the interaction with lattice phonons that cause population relaxation on a timescale determined by the spin-lattice relaxation time T_1. A spin-lattice relaxation time of 1.2 ms at room temperature was reported from NV ensemble measurements[24].

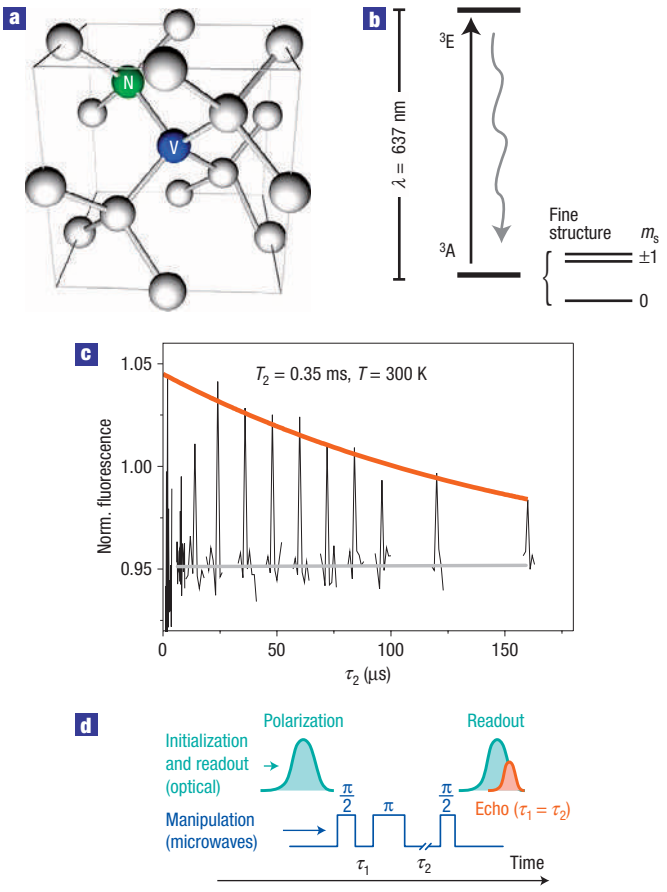

Figure 1 Structure, energy levels and coherence properties of single defects in diamond. a, Structure of the NV centre in diamond: the NV centre comprises a substitutional N centre, and a neighbouring vacancy. For our purposes we only deal with the negatively charged version of the centre. **b**, Abbreviated energy-level diagram of the NV centre showing fluorescence at 637 nm. ^{3}A and ^{3}E states represent the possible many-electron states corresponding to the symmetry group of the defect. **c**, Hahn echo decay curve of a single ^{14}NV electron spin (spin of NV centre with ^{14}N nitrogen isotope) recorded at room temperature. During each echo sequence, τ_1 was fixed and τ_2 was varied. Decoherence leads to a reduction of the echo amplitude as the pulse interval is increased. The orange curve is an exponential decay fit indicating a phase memory time of 350 μs. The grey line shows the fluorescence level corresponding to full loss of polarization providing a base line for the decay curve. **d**, Pulse sequence used for optical detection of the Hahn echo.

The existence of the long spin-coherence times for NV and N defects allows the observation of coherent coupling between defects, even in the limit of relatively weak coupling. Given a $T_2\sim0.35$ ms, two electron spins ($S=1/2$) should not be separated by more than 15 nm for their mutual interaction strength to be larger than the coupling to the bath of ^{13}C nuclei. Although single NV and N defects can be created one by one using single-ion implantation, the generation of pairs with intrapair spacings of only a few nanometres remains challenging, and must perforce

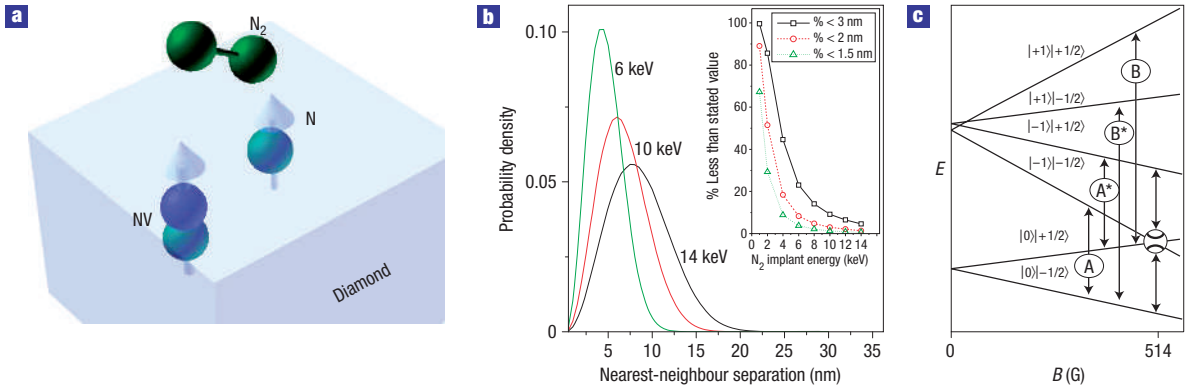

Figure 2 Generation of coupled spin pairs. a, Schematic diagram of molecular implantation leading to the formation of NV–N spin pairs. After entering the diamond, the chemical bond of the N_2^+ molecule is broken and the two N penetrate independently in the diamond. Hence, implantation of single N_2^+ ions leads to the formation of N–N pairs and vacancies (V) in the diamond substrate. Annealing leads to the conversion of some of the N into NV, leading to closely spaced NV–N pairs. **b**, Monte Carlo simulation of the distribution of intrapair spacings for implantations of 14-, 10- and 6-keV N_2^+ dimers. The inset shows the calculated fraction of implanted pairs with separations between the N defects less than 3, 2 and 1.5 nm as a function of N_2 implantation energy. **c**, Energy levels of a dipole–dipole coupled NV–N pair. The separation between the N states in the excited NV manifold at low B is the dipolar coupling, $\Delta = 13$ MHz, resolved in Fig. 3a.

be probabilistic. Two factors dominate the positioning accuracy. The first is the scattering of nitrogen ions in diamond during implantation (straggling). The second factor is the accuracy to which the ion beam can be focused. Current technology allows implantation of single ions[25], but the spatial implantation accuracy is limited to 20 nm (ref. 26). Implanting nitrogen molecules (N_2^+) rather than atoms (N^+) provides a solution to both problems (see Fig. 2a). Although absolute positioning accuracy is still limited by the beam focus, the relative accuracy (that is, the spacing between the two defects) is only affected by straggling. Figure 2b shows the distribution of intrapair spacings for implantations of 14-, 10- and 6-keV N_2 dimers obtained from Monte Carlo simulations using the Stopping and Range of Ions in Matter package[27,28]. The inset shows the fraction of implanted ions with intrapair separations less than 3, 2 and 1.5 nm as a function of N_2 implantation energy. Note that straggling can be minimized by decreasing the implantation energy resulting in an ever-increasing fraction of dimers with intrapair spacings in the regime likely to result in measurable coherent coupling. In the present work, 14-keV N_2 dimers were implanted. For this energy, the yield of pairs with N–N spacing of 2 nm or less is expected to be 1–2% of the implanted N_2 dimers.

After implanting two closely spaced nitrogen atoms using this molecular implantation technique the sample was annealed to form NV centres. With the implantation conditions used it was found that the conversion efficiency of N to NV was about 5%, as verified by the exclusive creation of ^{15}NVs when ^{15}N was implanted (the natural abundance of ^{15}N is 0.37%). This means that about 10% of the N_2 molecular implants were converted to an NV–N pair, leaving most of the rest as N–N pairs, consistent with the expected yield as described above. Owing to this low conversion efficiency of N into NV, no pairs of NV with sufficiently close spacing were observed (for details see the Methods section). As a result, we have concentrated our study on the NV–N pairs.

Evidence for NV–N coupling comes from ESR experiments. As the substitutional N defect is an electron spin 1/2 system, dipolar coupling between the two spins occurs. If the dipolar coupling is weak compared with the NV centre zero-field splitting and the Zeeman effect, perturbation theory can be applied to the description of the magnetic interactions between the two defects. The hamiltonian describing the coupled NV–N spin system is[29]

$$H = g_e\beta_e\hat{B}\hat{S}_1 + \hat{S}_1\hat{D}\hat{S}_1 + g_e\beta_e\hat{B}\hat{S}_2 + \hat{S}_1\hat{T}\hat{S}_2,$$

where g_e is the electronic g-factor, β_e is the Bohr magneton, $\hat{S}_1$, $\hat{S}_2$ are spin matrices corresponding to NV and N spins, respectively, $\hat{D}$ is the fine-structure tensor describing the interaction of the two uncoupled electron spins, and $\hat{T}$ is the magnetic dipolar interaction tensor. Eigenenergies of the coupled two-spin system as a function of external magnetic B field, shown in Fig. 2c, were obtained by diagonalizing the spin hamiltonian. Here, the six possible energy levels are identified by the spin quantum numbers of the individual defects (that is, $m_s = \pm 1/2$ for N and $m_s = 0, \pm 1$ for NV). According to the energy-level scheme, the splitting between doublet components of the NV $m_s = 0$ to ± 1 transitions corresponds to the dipole–dipole coupling strength and is expected to be $\Delta = 14$ MHz for a defect separation distance of 1.5 nm.

A typical ESR spectrum of a single NV–N spin pair produced by implanting $^{14}N_2$ is shown in the lower trace of Fig. 3a. As compared with an uncoupled defect (upper trace), the pairs show a line splitting into two sets of doublets. To demonstrate the coherent nature of the coupling, electron spin echo modulation experiments were used. In the spin Hahn echo measurements ($\pi/2 - \tau - \pi - \tau - \pi/2$-echo), the amplitude of the echo signal was measured as a function of the pulse separation τ. The $\pi/2$ and π pulses in both experiments were 15 and 30 ns, respectively. Therefore the bandwidth was larger than the splitting, allowing full excitation of the ESR doublet (AA* transition shown in Fig. 3a). The echo envelope shows periodic oscillation (electron spin echo envelope modulation, ESEEM, Fig. 3b). The mechanism responsible for the oscillations observed is the inclusion of pseudosecular dipole–dipole couplings between NV and N spins. For the current situation where the strength of dipole–dipole coupling is comparable to the difference of Zeeman terms $|\omega_{D-D}| \sim |\omega_1^{Zeeman} - \omega_2^{Zeeman}|$, pseudosecular terms in the coupling are non-vanishing and can be written as $A_{SX}S_{1Z}S_{2X}$. As a result, during the echo sequence the spin of the NV centre precesses with different frequencies before and after the π pulse. Thus, the phase acquired by the NV spin is

not cancelled by refocusing and results in the periodic oscillation of the echo amplitude[30,31]. From a Fourier transformation of the oscillation pattern, the NV–N coupling frequency is obtained, which agrees with that observed in the ESR spectrum of Fig. 3a. The observation of the echo modulation pattern is an unambiguous demonstration of coherent coupling. The Hahn echo modulation in Fig. 3b shows not only the NV–N coupling frequency which corresponds to NV–N coupling, but also satellites corresponding to the internal hyperfine coupling[32] associated with the ^{14}N nucleus. Finally, it is important to note that no decay of the echo is visible within the measurement time interval.

Only the NV centre couples to the optical field, and hence optical initialization can only be applied to the NV centre. A symmetric shape of the ESR doublet in Fig. 3a indicates that the states $|0\rangle|+(1/2)\rangle$ and $|0\rangle|-(1/2)\rangle$ are populated equally under normal conditions. To polarize (that is, initialize) the nitrogen spin, resonant spin flip-flop processes induced by dipolar coupling between the NV and N were exploited. As the spin flip-flop is energy conserving, it is suppressed when the spins are not energetically equivalent, which occurs at most magnetic fields in the NV–N system (see Fig. 4a). To achieve polarization transfer, the frequencies of NV and N spin transitions were tuned into mutual resonance by applying a magnetic field of $B = 514$ G along the symmetry axis of the NV defect. Exact degeneracy is given at the point of level anticrossing $B = 514$ G (see circled anticrossing in Fig. 2c).

The lower graph of Fig. 4a demonstrates this polarization transfer by showing what happens to the ESR spectra (transitions AA* in the energy-level scheme presented in Fig. 2c) when the applied magnetic field is tuned through the mutual resonance condition. The disappearance of the high-frequency A* component of the ESR spectrum at mutual resonance, 514 ± 20 G, is evidence of spin polarization of the N defect. This occurs because of mutual NV–N spin flips, between states $|0\rangle|+(1/2)\rangle$ and $|-1\rangle|-(1/2)\rangle$, followed by selective optical pumping of the NV. The timescale for the polarization is given by the coupling strength between NV and N ($\Delta = 14$ MHz) and the optical pumping rate (1.8 MHz). Note that the sample relevant for this experiment was implanted with $^{15}N_2^+$ and ^{15}NV–^{15}N pairs were created.

The width of the polarization transfer resonance is expected to be limited by the homogeneous linewidth of both spin transitions, that is, of the kHz order. However, under continuous optical illumination, the resonance of the NV centre broadens because optical pumping disturbs the spin coherence: hence, polarization transfer occurs over a wide magnetic field range because of the overlap between the tails of the resonance lines. To describe the build up of N polarization we used a model including dipolar coupling (Δ), spin-lattice relaxation of nitrogen and NV spins (γ_{SL}^{N}, γ_{SL}^{NV}) and optical pumping acting on NV spins (γ_{opt}^{NV}). The mutual spin flip-flop rate was calculated as a product of dipolar coupling ($\Delta = 14$ MHz in the presented case) and the overlap integral F between NV and N lineshapes[33] $F = 1/[1+[D/2(\gamma^{N}+\gamma^{NV})]^2]$. Here γ^{N} and γ^{NV} are the dephasing rates of N and NV spins, and D is the detuning between ESR lines, respectively. The result of the calculation without any fitting parameters together with experimental data is shown in Fig. 4b. Note that the optical polarization and coherence times of the NV centre were measured independently in pulsed ESR experiments.

A detailed examination of the ESR spectra reveals not only the disappearance of the high-frequency component of the ESR doublet, but also an asymmetric narrowing of the spectral lines close to NV–N mutual resonance (Fig. 4a). This narrowing is related to the build up of nuclear polarization of NV centre. As the sample used for Fig. 4 was implanted with ^{15}N isotopes, each ESR line consists of two hyperfine transitions associated with the ^{15}N nuclei of the NV. Those components are not well resolved in the optically detected magnetic resonance spectra presented in Fig. 4a because of line broadening associated with optical pumping. To observe this nuclear polarization, Fig. 4c shows ESR spectra recorded at low optical excitation power. The

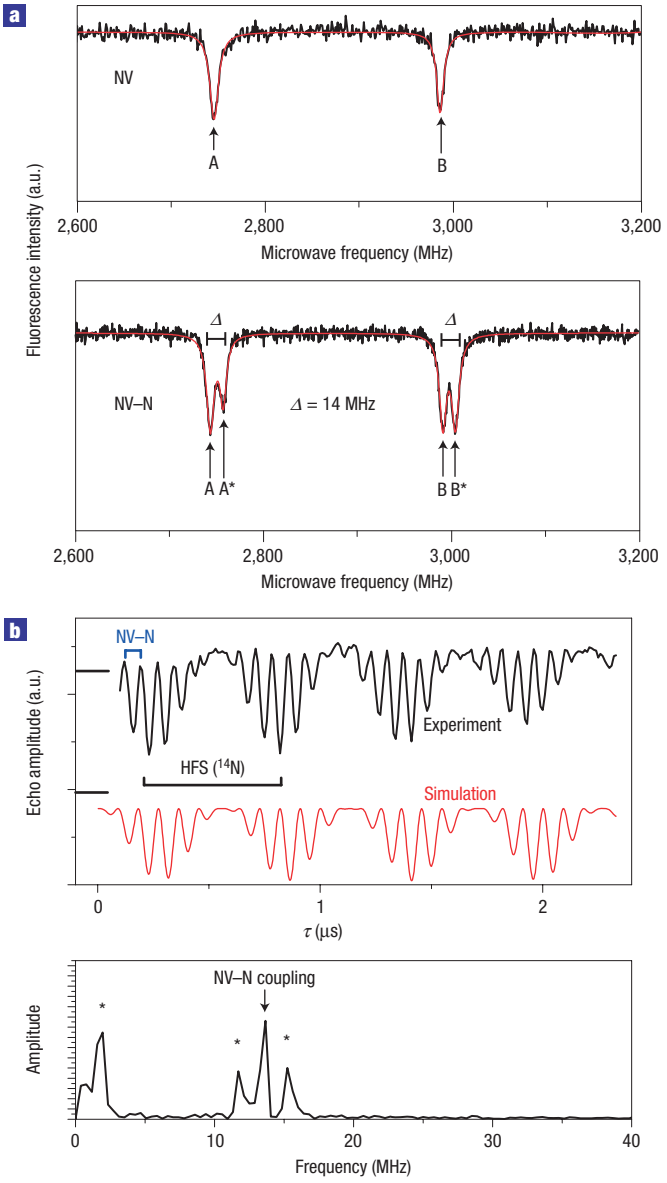

Figure 3 Magnetic resonance on NV–N spin pairs. a, Optically detected electron spin resonance spectrum of a single ^{14}NV–^{14}N pair in a weak magnetic field (40 G). The upper graph shows the ESR spectrum of a single NV centre, showing only two transitions from $m_s = 0$ to the $m_s = +1$ and -1 spin states (A and B). Dipolar coupling between the NV and N leads to the doublets (A, A* and B, B* transitions shown in the lower graph). **b**, Hahn echo modulation and its Fourier transformation showing coupling between the two spins. The lower (red) graph shows simulation of the ESEEM pattern based on dipolar interactions between NV–N electron spins and the hyperfine interaction with the ^{14}N nucleus. The modulation depth of the echo corresponds to 85% of the Rabi oscillation amplitude indicating the presence of a pseudosecular part in the effective interaction hamiltonian. The coupling strength between N and NV electron spins is indicated by the peak at around 13 MHz. The asterisks indicate frequencies associated with the ^{14}N hyperfine structure (HFS). The Hahn sequence was carried out in a static magnetic field of 50 G.

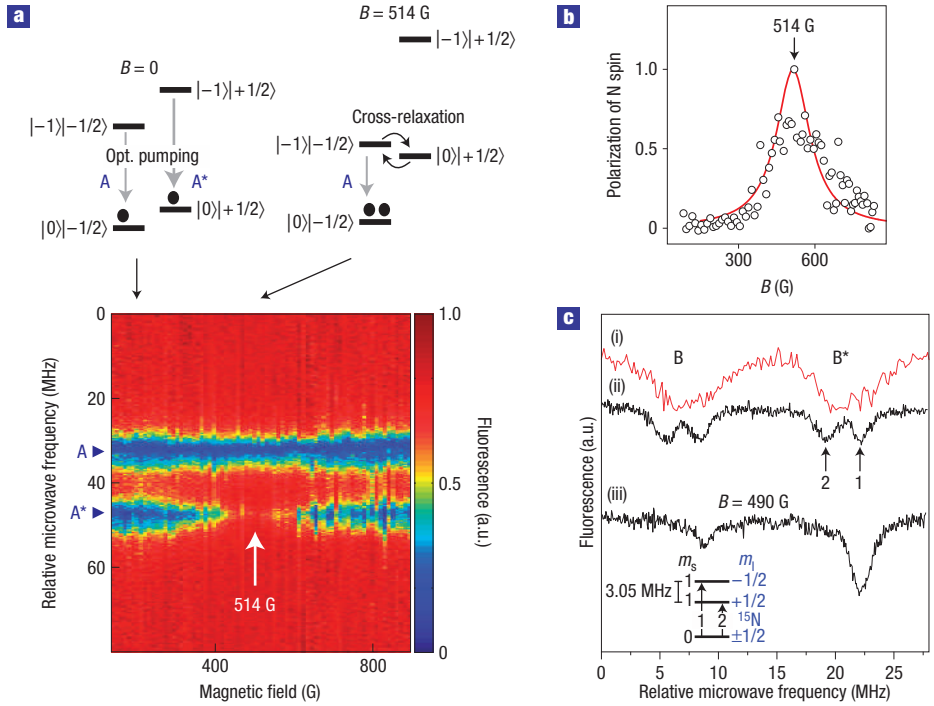

Figure 4 Polarization transfer between coupled NV–N electron spins and build-up of the polarization of a ^{15}N nuclear spin. a, Evolution of ESR doublet AA* on varying the external magnetic field. The level diagrams at the top show the coupled spin levels at two magnetic fields to illustrate how the N electron spin is polarized by means of dipolar coupling to the optically pumped NV centre. **b**, Polarization P of the N electron spin as a function of applied magnetic field. Polarization is defined as $P=(I_A-I_{A^*})/(I_A+I_{A^*})$, where I_{A^*}, I_A are the intensities of the corresponding ESR spectrum components. The solid red line represents the unfitted model described in the text. The parameters for this model are: $\Delta = 14$ MHz, $\gamma_{opt}^{NV} = 1.8$ MHz, $\gamma_{SL}^{NV} = 1$ kHz and $\gamma_{SL}^{N} = 1/3$ kHz (see the Methods section for details). **c**, Curves (i) and (ii) show high-resolution ESR spectra of a ^{15}NV–^{15}N pair (only transitions B and B* are shown). Each transition shows hyperfine structure (transition 1 and 2 are shown in the inset) associated with the ^{15}N nuclei. Curve (i) is measured with high laser power, so the lines are broadened and no hyperfine structure is visible. Curve (ii) is measured with lower laser power to clearly resolve the hyperfine spectrum. In curve (iii), one of the hyperfine components is not visible when the system is excited at the mutual energetic resonance frequency of the NV and N electron spins, indicating the build up of the spin polarization of the ^{15}N.

disappearance of one of the hyperfine transition lines is evidence of the polarization of the ^{15}N nuclear spin. By analogy to the N electron polarization by mutual interaction with the NV, this nuclear polarization occurs by 'flip-flop' processes involving the simultaneous spin flip of the nuclear and optically aligned electron spins. This single-atom experiment is similar to the nuclear cooling scheme recently demonstrated for quantum dots[34]. Here it serves to initialize a three-coupled-spin system consisting of two electrons and one nucleus.

In conclusion, we demonstrate room-temperature optical initialization and readout of a coupled two-electron-spin system in diamond. The system is potentially scalable to a large number of spins pending the future development of higher resolution implanting techniques. This is a first step towards the development of room-temperature solid-state quantum computing and long-distance quantum communication devices. Much of the potential usefulness of this NV diamond system for solid-state quantum information processing lies in the optical accessibility of long-lived electron and nuclear spin states, even at room temperature. Additional advantages arise from the ability to manipulate the spin states with advanced ESR techniques, such as composite pulses[35,36] to potentially achieve exquisite control. The manipulation of single spins in this system has already been demonstrated[3,5]. From the long spin coherence demonstrated in the present work, we estimate that 10^4 Rabi flops can be accomplished before decoherence at room temperature occurs (this factor is at least 10^2 for coupled spins).

METHODS

CREATION OF NV AND N CENTRES IN DIAMOND BY ION IMPLANTATION

To create NV centres in type IIa diamonds (nitrogen concentration <0.1 p.p.m.), we implanted 14-keV N^+ ions or N_2^+ ions with a dose of $\sim 2\times10^9$ cm^{-2} and annealed the sample for 1 h in an Ar atmosphere at 900 °C. This procedure led to the formation of NV–N pairs with a yield of approximately 1%. For liquid nitrogen substrate implantation temperature the yield is close to 10%. The hyperfine structure of the ESR spectra was in agreement with the implanted N isotope (^{14}N or ^{15}N), indicating that only the implanted nitrogen, and not traces of residual nitrogen present in the sample, were responsible for the formation of NV–N pairs.

OPTICALLY DETECTED MAGNETIC RESONANCE ON SINGLE SPINS

Optical detection of single NV–N pairs was carried out with a 532-nm excitation wavelength using a lab-built confocal microscope. To ensure that the optical signal originated from a single NV–N pair, the second-order intensity autocorrelation function was measured and the antibunching dip was observed to reach zero at zero delay time. The contrast of the antibunching dip is expected to be 0.5 for two NV centres (this case was not usually observed experimentally because of the low formation yield of NV centre). N–N pairs were not detectable (note that N defect is not active in fluorescence). For magnetic resonance measurements, the sample was mounted on a miniaturized loop connected to a 40-W travelling wave tube amplifier. The results presented in this paper were obtained for ^{14}NV–^{14}N (Fig. 3) and ^{15}NV–^{15}N (Fig. 4) spin pairs. The strength and orientation of the applied magnetic field was calibrated using the level anticrossing resonance of the NV centre at 1,028 G.

As scattering of photons provides information about the spin state of the system, optical illumination led to decoherence related to projective

measurement. To avoid this effect, spin manipulation was carried out under dark conditions. The system was polarized into the $m_s = 0$ sublevel by strong non-selective illumination (laser pulse of 3-μs duration and 5×10^8 W m^{-2} intensity). After that, the laser was switched off and the microwave pulse sequence applied. The typical π pulse duration was 30 ns for 20-W microwave output power. The readout of the spin state was achieved by monitoring the fluorescence intensity using a readout laser pulse.

HAHN ECHO MEASUREMENTS

The conventional Hahn echo sequence $\pi/2 - \tau - \pi - \tau$ (comprises $\pi/2$ and π microwave pulses and waiting times τ) is a classical method for measuring the spin-coherence time. Initially the system was prepared in $m_s = 0$ spin state. The first $\pi/2$ pulse creates a coherent superposition of $m_s = 0$ and 1 (or -1) states. During free evolution time τ between the first and second pulses, the spin freely evolves. The second π pulse inverts the direction of evolution of the spin. After a second waiting time τ, the magnetization vectors are in phase and a primary echo is observed. Decoherence processes related to loss of phase of the spin superposition induce decay of the echo amplitude. The main advantage of the echo technique compared with the free induction decay is the ability to eliminate the experimental artefacts related to the temporal instability of the magnetic field. In our experiments the classical two-pulse Hahn echo sequence was adopted to optically detect magnetic resonance by introducing an additional $\pi/2$ pulse at the end to convert the final spin coherence into populations, measurable by fluorescence detection. For interacting spins, the spin-echo pulse sequence rephases the spin coupling in a time-independent hamiltonian. In ESEEM, the NV electron's dipolar field tilts the quantization axis of the second N spin which then affects the NV electron. This coherent coupling results in a time-oscillatory hamiltonian, which, when subjected to a spin-echo pulse sequence, gives a modulation of the electron spin echo envelope. This shows that two spins are coherently coupled and are located in close proximity.

The experiments were time averaged for 10^5–10^6 cycles to obtain smooth curves and to allow for a comparison with theory. Such long averaging was the limiting factor in the measurements of echo modulation for the coupled system, where fine time sampling was required.

POLARIZATION TRANSFER BETWEEN NV AND N SPINS

To calculate the dependence of N polarization on the magnetic field strength, a system of rate equations was used taking into account the transitions between the following states, (1): $|0\rangle|-1/2\rangle$, (2): $|0\rangle|+1/2\rangle$, (3): $|-1\rangle|-1/2\rangle$ and (4): $|-1\rangle|+1/2\rangle$. The rate of flip-flop process δ depends on the overlap integral F and coupling strength Δ as $\delta = F \cdot \Delta$ (see the text for the expression of F). The steady-state solution of the following set of equations was used to model the polarization of the N electron spin.

$$\frac{\partial}{\partial t}\begin{bmatrix} n_1 \\ n_2 \\ n_3 \\ n_4 \end{bmatrix} = \begin{bmatrix} -\gamma_{SL}^{N} - \gamma_{SL}^{NV} & \gamma_{SL}^{N} & \gamma_{opt}^{NV} + \gamma_{SL}^{NV} & 0 \\ \gamma_{SL}^{N} & -\delta - \gamma_{SL}^{N} - \gamma_{SL}^{NV} & \delta & \gamma_{opt}^{NV} + \gamma_{SL}^{NV} \\ \gamma_{SL}^{NV} & \delta & -\delta - \gamma_{SL}^{N} - \gamma_{SL}^{NV} - \gamma_{opt}^{NV} & \gamma_{SL}^{N} \\ 0 & \gamma_{SL}^{NV} & \gamma_{SL}^{N} & -\gamma_{opt}^{NV} - \gamma_{SL}^{N} - \gamma_{SL}^{NV} \end{bmatrix} \bullet \begin{bmatrix} n_1 \\ n_2 \\ n_3 \\ n_4 \end{bmatrix}.$$

The parameters needed to evaluate these equations were determined as follows. The rate of optical pumping γ_{opt}^{NV} was measured in a pulsed experiment by first starting in the $m_s = 0$ state, then applying a single microwave π pulse to transfer population into the $m_s = -1$ sublevels. During the subsequent illumination the fluorescence starts at a low level and increases to its initial high level as the system is polarized back into the $m_s = 0$ sublevels with a time constant of 570 ns. This gives γ_{opt}^{NV}, which also determines the coherence time of the NV centre under illumination. The spin-lattice relaxation time of N and NV centres (3 and 1 ms, respectively)[9,19] as well as the coherence time of N (1 ms)[37] were taken from the literature. Finally, the detuning D was derived from the ESR spectra allowing us to calculate F and δ.

Received 20 March 2006; accepted 2 May 2006; published 28 May 2006.

References

1. Li, X. Q. *et al.* An all-optical quantum gate in a semiconductor quantum dot. *Science* **301,** 809–811 (2003).
2. Hettich, C. *et al.* Nanometer resolution and coherent optical dipole coupling of two individual molecules. *Science* **298,** 385–389 (2002).
3. Jelezko, F., Gaebel, T., Popa, I., Gruber, A. & Wrachtrup, J. Observation of coherent oscillations in a single electron spin. *Phys. Rev. Lett.* **92,** 076401 (2004).
4. Gruber, A. *et al.* Scanning confocal optical microscopy and magnetic resonance on single defect centers. *Science* **276,** 2012–2014 (1997).
5. Jelezko, F. *et al.* Observation of coherent oscillation of a single nuclear spin and realization of a two-qubit conditional quantum gate. *Phys. Rev. Lett.* **93,** 130501 (2004).
6. Howard, M. *et al.* Quantum process tomography and Linblad estimation of a solid-state qubit. *New J. Phys.* **8,** 33 (2006).
7. Wrachtrup, J. & Jelezko, F. Quantum information processing in diamond. *J. Phys. Condens. Matter* **18,** S807–S824 (2006).
8. Greentree, A. D. *et al.* Critical components for diamond-based quantum coherent devices. *J. Phys. Condens. Matter* **18,** S825–S842 (2006).
9. Beveratos, A. *et al.* Single photon quantum cryptography. *Phys. Rev. Lett.* **89,** 187901 (2002).
10. Olivero, P. *et al.* Ion-beam-assisted lift-off technique for three-dimensional micromachining of freestanding single-crystal diamond. *Adv. Mater.* **17,** 2427–2430 (2005).
11. Greentree, A. D., Salzman, J., Prawer, S. & Hollenberg, L. C. L. Quantum gate for Q switching in monolithic photonic-band-gap cavities containing two-level atoms. *Phys. Rev. A* **73,** 013818 (2006).
12. Tomljenovic-Hanic, S., Steel, M. J., Sterke, C. M. d. & Salzman, J. Diamond based photonic crystal microcavities. *Opt. Express* **14,** 3556–3562 (2006).
13. Kennedy, T. A., Colton, J. S., Butler, J. E., Linares, R. C. & Doering, P. J. Long coherence times at 300 K for nitrogen-vacancy center spins in diamond grown by chemical vapor deposition. *Appl. Phys. Lett.* **83,** 4190–4192 (2003).
14. Epstein, R. J., Mendoza, F. M., Kato, Y. K. & Awschalom, D. D. Anisotropic interactions of a single spin and dark-spin spectroscopy in diamond. *Nature Phys.* **1,** 94–98 (2005).
15. Meijer, J. *et al.* Generation of single color centers by focused nitrogen implantation. *Appl. Phys. Lett.* **87,** 261909 (2005).
16. Rabeau, J. R. *et al.* Implantation of labelled single nitrogen vacancy centers in diamond using ^{15}N. *Appl. Phys. Lett.* **88,** 023113 (2006).
17. Goss, J. P. *et al.* Comment on "Electronic structure of the N-V center in diamond: Theory". *Phys. Rev. B* **56,** 16031–16032 (1997).
18. He, X. F., Manson, N. B. & Fisk, P. T. H. Paramagnetic-resonance of photoexcited N-V defects in diamond. II. Hyperfine interaction with the N-14 nucleus. *Phys. Rev. B* **47,** 8816–8822 (1993).
19. Manson, N. B., Harrison, J. P. & Sellars, M. J. The nitrogen-vacancy in diamond revisited. Preprint at <http://arxiv.org/abs/cond-mat/0601360> (2006).
20. Kennedy, T. A. *et al.* Single-qubit operations with the nitrogen-vacancy center in diamond. *Phys. Status Solidi B* **233,** 416–426 (2002).
21. Hoch, M. J. R. & Reynhardt, E. C. Nuclear-spin-lattice relaxation of dilute spins in semiconducting diamond. *Phys. Rev. B* **37,** 9222–9226 (1988).
22. Khutsish, G. Spin diffusion. *Sov. Phys. Uspekhi-USSR* **8,** 743 (1966).
23. de Sousa, R. & Das Sarma, S. Theory of nuclear-induced spectral diffusion: Spin decoherence of phosphorus donors in Si and GaAs quantum dots. *Phys. Rev. B* **68,** 115322 (2003).
24. Redman, D. A., Brown, S., Sands, R. H. & Rand, S. C. Spin dynamics and electronic states of N-V centers in diamond by EPR and four-wave-mixing spectroscopy. *Phys. Rev. Lett.* **67,** 3420–3423 (1991).
25. Persaud, A. *et al.* Single ion implantation with scanning probe alignment. *J. Vac. Sci. Technol. B* **22,** 2992–2994 (2004).
26. Jamieson, D. N. *et al.* Controlled shallow single-ion implantation in silicon using an active substrate for sub-20-keV ions. *Appl. Phys. Lett.* **86,** 202101 (2005).
27. Ziegler, J. F. *The Stopping and Range of Ions in Matter* (Pergamon, New York, 1977–1985).
28. Wilson, H. F. *et al.* P2 Dimer implantation in silicon: a molecular dynamics study. *Nucl. Instrum. Methods Phys. Res. B* (2006) in the press.
29. Vanoort, E., Stroomer, P. & Glasbeek, M. Low-field optically detected magnetic-resonance of a coupled triplet-doublet defect pair in diamond. *Phys. Rev. B* **42,** 8605–8608 (1990).
30. Schweiger, A. & Jeschke, G. *Principles of Pulse Electron Paramagnetic Resonance* (Oxford Univ. Press, Oxford, 2001).
31. Kalin, M. & Schweiger, A. Radio-frequency-driven electron spin echo envelope modulation spectroscopy on spin systems with isotropic hyperfine interactions. *J. Chem. Phys.* **115,** 10863–10875 (2001).
32. Charnock, F. T. & Kennedy, T. A. Combined optical and microwave approach for performing quantum spin operations on the nitrogen-vacancy center in diamond. *Phys. Rev. B* **64,** 041201 (2001).
33. Abragam, A. *Principles of Nuclear Magnetism* (Clarendon, Oxford, 1961).
34. Lai, C. W., Maletinsky, P., Badolato, A. & Imamoglu, A. Knight-field-enabled nuclear spin polarization in single quantum dots. *Phys. Rev. Lett.* **96,** 167403 (2006).
35. Cummins, H. K., Llewellyn, G. & Jones, J. A. Tackling systematic errors in quantum logic gates with composite rotations. *Phys. Rev. A* **67,** 042308 (2003).
36. Morton, J. J. L. *et al.* High fidelity single qubit operations using pulsed electron paramagnetic resonance. *Phys. Rev. Lett.* **95,** 200501 (2005).
37. van Wyk, J. A., Reynhardt, E. C., High, G. L. & Kiflawi, I. The dependences of ESR line widths and spin-spin relaxation times of single nitrogen defects on the concentration of nitrogen defects in diamond. *J. Phys. D* **30,** 1790–1793 (1997).

Acknowledgements

This work was supported by DFG (project SFB/TR 21), EU (Integrated Project Qubit Applications—QAP—funded by the IST directorate as Contract Number 015848) and 'Landesstiftung B-W' (project 'Atomoptik'). The single-ion implantation work was supported by the Australian Research Council, the Australian Government, and the US National Security Agency (NSA), Advanced Research and Development Activity (ARDA), and the Army Research Office (ARO) under contract numbers W911NF-04-1-0290 and W911NF-05-1-0284, and DARPA QuIST under AFOSR contract number C02-00060. We thank G. Tamanyan for technical assistance with the implantations. Correspondence and requests for materials should be addressed to F.J. or J.W.

Competing financial interests

The authors declare that they have no competing financial interests.